Progress In Electromagnetics Research B, Vol. 26, 335–359, 2010

REALISTIC MODEL OF DISPERSIVE SOILS USING PLRC-FDTD WITH APPLICATIONS TO GPR SYSTEMS

G. E. Atteia

Electronics and Communications Engineering Department
Zagazig University, Egypt

K. F. A. Hussein

Microwave Engineering Department
Electronics Research Institute (ERI), Cairo, Egypt

Abstract—A realistic model of ground soil is developed for the electromagnetic simulation of Ground Penetrating Radar (GPR) systems. A three dimensional Finite Difference Time Domain (FDTD) algorithm is formulated to model dispersive media using N-term Debye permittivity function with static conductivity. The formulation of the algorithm is based on the concept of the Piecewise Linear Recursive Convolution (PLRC) in order to simulate the dispersion properties of soil as a two-term Debye medium. This approach of ground modeling enhances the accuracy and reliability of results obtained for GPR problems. The developed algorithm is validated when simulating practical GPR Systems used to detect different objects buried in Puerto-Rico and San Antonio clay loams. The proposed algorithm is employed to compare the impact of using two-term Debye model to simulate real soil on the coupling coefficient between transmitting and receiving antennas due to the absence and presence of buried targets to that of using non-dispersive soil model. The effect of soil moisture content on the performance of GPR system in detecting buried objects such as metallic and plastic pipes is investigated.

Received 31 August 2010, Accepted 24 October 2010, Scheduled 1 November 2010
Corresponding author: Ghada Emam Atteia (gemhmd@yahoo.com).

1. INTRODUCTION

Recently, there have beem considerable efforts devoted to compute propagation through linear dispersive media using FDTD method because the standard FDTD scheme introduced by Yee [1] is typically implemented with constant values of permittivity and conductivity which is serious limitation. Using the standard FDTD version is only valid for narrow frequency band applications, but cannot be used for those employ materials with significant frequency dependence constitutive parameters. A wide variety of media in nature such as water, soil, human tissues and plasma have frequency dependent properties when it interacts with electromagnetic waves. However, many papers in the literature [2–5] use the original FDTD algorithm for solving electromagnetic waves interaction with such materials regardless of its dispersive nature in GPR frequency range. In consequence, the obtained results are not accurate as they should be. Seriously, using such unspecialized method in biomedical applications such as hyperthermia or cancer detection may give false results which could be hazardous when it is related with urgent medical decision. Therefore, many approaches have been conducted to modify existing FDTD algorithm to take into consideration the frequency-dependence properties of dispersive media [6]. The Z-transform is applied by Sullivan in [7] to Maxwell equations to develop a formulation suitable for dispersive media. An alternative approach involving the addition of an auxiliary difference equation (ADE) that relates the electric flux density to the electric field intensity to the FDTD is presented in [8–10]. Other technique called the Recursive convolution (RC) was developed in [11, 12].This method was the most efficient method in terms of saving computer time and storage. The principle of RC technique is the recursive evaluation of the discrete convolution resulting from the Fourier transform of two frequency-dependent functions ($E(\omega)$ and $\varepsilon(\omega)$). Two improvements were developed in [13] to meet the requirements of transient electromagnetic propagation computation in plasma including dealing with frequencies where plasma permittivity is negative. It was also used to simulate hyperthermia treatment with a broad band applicator presented in [14]. The disadvantage of this method is the inaccuracy of obtained results compared with results from the previous two approaches. Later, greater accuracy was achieved by a modified version of the RC technique called the Piecewise Linear Recursive Convolution (PLRC) technique [15]. The main difference between these two techniques(RC and PLRC) is that the former assumes a constant electric field over each time step while the later assumes that the electric field has a piecewise linear function

dependence over (Δt) as will be shown later in this section.

The PLRC method in [15] is used in this paper to solve Maxwell's equation in linear dispersive media (Ground soil) described by Debye model with static conductivity in a simple GPR problem. Noteworthy that the PLRC method described in [15] was developed for single Debye and Lorentz pole type linear media that, a one-term Debye relaxation equation is often not enough and multi-term Debye relaxation equations must therefore be used to describe the dispersion characteristics of ground soil [16]. Therefore, efforts have been dedicated to incorporate soil dispersion of multiterm Lorentz or Debye models into the FDTD scheme [17]. This is done in [18] using PLRC based on the split field form of Maxwell's equations. Moreover the ADE method is used in [20] to model soils for real GPR environment.

In this paper, the PLRC method is extended for N-term Debye media to introduce the use of two-term Debye model for more realistic simulation of real ground soil. This modification is derived in the similar way described in [12] for the formulation of the RC-method for N-order Lorentz media but using the principles of the PLRC for N-term Debye media instead of that of the original RC method. This choice is based on the accuracy provided by the PLRC method that rival that of ADE and Z-transform approaches and retain the efficiency of RC method in saving computer time and storage requirements.

2. FORMULATION OF THE FDTD UPDATE EQUATIONS

Starting with Maxwell's equations in time domain:

$$\nabla \times \vec{E} = -\frac{\partial \vec{B}}{\partial t} \tag{1}$$

$$\nabla \times \vec{H} = \frac{\partial \vec{D}}{\partial t} + \sigma \vec{E} \tag{2}$$

Recalling the relationship between D and E in the frequency domain

$$D(\omega) = \varepsilon_o \varepsilon(\omega) E(\omega), \tag{3}$$

where,

$$\varepsilon(\omega) = \varepsilon_\infty + \chi(\omega), \tag{4}$$

and ε_o is the permittivity of free space, $\chi(\omega)$ is the Fourier transform of the electric susceptibility $\chi(\tau)$ and ε_∞ is the infinite frequency permittivity. By substituting from (4) into (3) and taking the inverse Fourier transform for the resulting equation, we find

$$D(t) = \varepsilon_o \varepsilon_\infty E(t) + \varepsilon_o \chi(\tau) * E(t) \tag{5}$$

The convolution appearing in (5) results from taking the inverse Fourier transform of the product $\chi(\omega)E(\omega)$.

Equation (5) can be rewritten as

$$D(t) = \varepsilon_o \varepsilon_\infty E(t) + \varepsilon_o \int_0^t E(t-\tau)\chi(\tau)d\tau \tag{6}$$

Equation (6) can be rewritten in a discrete-time form as follows

$$D^n = \varepsilon_o \varepsilon_\infty E^n + \varepsilon_o \int_0^{n\Delta t} E(n\Delta t - \tau)\chi(\tau)d\tau, \tag{7}$$

where $\triangle t$ is an incremental time step and n is the discrete time index.

For PLRC, the electric field is assumed to have a piecewise linear dependence over Δt [15] as follows

$$E(t) = E^n + \frac{E^{n+1} - E^n}{\Delta t}(t - n\Delta t) \tag{8}$$

Using the piecewise linear relation (8) for the electric field and substituting into (7), one gets

$$E(n\Delta t - \tau) = E^{n-m} + \frac{E^{n-m-1} - E^{n-m}}{\Delta t}(\tau - m\Delta t) \tag{9}$$

Substituting by (9) into (7)

$$D^n = \varepsilon_o \varepsilon_\infty E^n + \varepsilon_o \sum_{m=0}^{n-1} \left\{ E^{n-m}\chi^m + \left(E^{n-m-1} - E^{n-m}\right)\xi^m \right\} \tag{10}$$

where,

$$\chi^m = \int_{m\Delta t}^{(m+1)\Delta t} \chi(\tau)d\tau \tag{11}$$

$$\xi^m = \frac{1}{\Delta t} \int_{m\Delta t}^{(m+1)\Delta t} \chi(\tau)(\tau - m\Delta t)d\tau \tag{12}$$

Utilizing Ampere's law in discrete-time form and making use of (10), one can get the following update equation for the electric field.

$$\nabla \times H^{n+\frac{1}{2}} = \frac{D^{n+1} - D^n}{\Delta t} + \sigma E^{n+1} \tag{13}$$

Now, the general form of the FDTD electric field update equation in linear dispersive medium becomes

$$E^{n+1} = \frac{\varepsilon_\infty - \xi^o}{\varepsilon_\infty + \frac{\sigma\Delta t}{\varepsilon_o} + \chi^o - \xi^o} E^n + \frac{\Delta t}{\varepsilon_o \left(\varepsilon_\infty + \frac{\sigma\Delta t}{\varepsilon_o} + \chi^o - \xi^o\right)} \nabla \times H^{n+\frac{1}{2}}$$

$$+ \frac{1}{\varepsilon_\infty + \frac{\sigma\Delta t}{\varepsilon_o} + \chi^o - \xi^o} \sum_{m=0}^{n-1} \left\{ E^{n-m} \Delta\chi^m + (E^{n-m-1} - E^{n-m}) \Delta\xi^m \right\} \quad (14)$$

where,

$$\Delta\chi^m = \chi^m - \chi^{m+1} \quad (15)$$

$$\Delta\xi^m = \xi^m - \xi^{m+1} \quad (16)$$

The convolution summation in (14) for a complex permittivity with a N-pole Debye model could be evaluated recursively. This is possible since the time-domain susceptibility function $\chi(\tau)$ is an exponential function of time (for each pole) as proved in [11–13]. The summation in (14) is called the recursive accumulator ψ^n

$$\psi^n = \sum_{m=0}^{n-1} \left\{ E^{n-m} \Delta\chi^m + \left(E^{n-m-1} - E^{n-m}\right) \Delta\xi^m \right\} \quad (17)$$

The recursion relation for the quantity ψ^n can be derived for Debye media and has the form

$$\psi^n = \sum_{p=1}^{N} \psi_p^n = \sum_{p=1}^{N} \left(\left(\Delta\chi_p^o - \Delta\xi_p^o\right) E^n + \Delta\xi_p^o E^{n-1} + C_{rec} \psi_p^{n-1} \right) \quad (18)$$

where ψ_p^n is the recursive accumulator of the pth pole. As shown in the next section, the constants $\Delta\chi_p^o$, $\Delta\xi_p^o$ and C_{rec} depend on the susceptibility function of the dispersive model used to describe the frequency dependence of the dispersive medium (as Debye, Drude or Lorentz media). With substituting by the recursive accumulator ψ^n into (14), the final form of the electric field update equation becomes

$$E^{n+1} = \frac{\varepsilon_\infty - \xi^o}{\varepsilon_\infty + \frac{\sigma\Delta t}{\varepsilon_o} + \chi^o - \xi^o} E^n + \frac{\Delta t}{\varepsilon_o \left(\varepsilon_\infty + \frac{\sigma\Delta t}{\varepsilon_o} + \chi^o - \xi^o\right)} \nabla \times H^{n+\frac{1}{2}}$$

$$+ \frac{1}{\varepsilon_\infty + \frac{\sigma\Delta t}{\varepsilon_o} + \chi^o - \xi^o} \psi^n \quad (19)$$

2.1. Recursive Convolution for N-term Debye Media

Debye media are characterized by a susceptibility or, equivalently, permittivity Function that has one or more real poles at separate

frequencies. The susceptibility function of N-term Debye media is given by

$$\chi(\omega)=\sum_{p=1}^{N}\frac{A_p}{(1+j\omega\tau_p)}=\frac{A_1}{(1+j\omega\tau_1)}+\frac{A_2}{(1+j\omega\tau_2)}+\frac{A_3}{(1+j\omega\tau_3)}+\ldots \quad (20)$$

where A_p is the pole amplitude and τ_p is the relaxation time of the pth pole.

In order to describe practically the dispersion in real ground soil, the frequency dependence of practical soil requires higher order Debye model. In the present study the dispersive ground properties are considered to follow the two-term Debye media as it is the best real implementation of practical ground soil [16].

For a Debye medium with N-natural frequencies, the inverse Fourier transform of the complex susceptibility function in (20) can be written as

$$\chi(t)=\sum_{p=1}^{N}\frac{A_p}{\tau_p}e^{-\frac{t}{\tau_p}}u(t)=\left(\frac{A_1}{\tau_1}e^{-\frac{t}{\tau_1}}+\frac{A_2}{\tau_2}e^{-\frac{t}{\tau_2}}+\frac{A_3}{\tau_3}e^{-\frac{t}{\tau_3}}+\ldots\right)u(t) \quad (21)$$

Substituting from (21) into (11) and (12) yields

$$\chi^m=\sum_{p=1}^{N}\chi_p^m=\sum_{p=1}^{N}A_p\left[1-e^{-\frac{\Delta t}{\tau_p}}\right]e^{\frac{-m\Delta t}{\tau_p}} \quad (22)$$

$$\xi^m=\sum_{p=1}^{N}\xi_p^m=\sum_{p=1}^{N}-A_p\frac{\tau_p}{\Delta t}\left[e^{-\frac{\Delta t}{\tau_p}}\left(\frac{\Delta t}{\tau_p}+1\right)-1\right]e^{\frac{-m\Delta t}{\tau_p}} \quad (23)$$

At $m=0$, the parameters χ^o and ξ^o required in the electric field update Equation (19) are the summation of χ_p^o and ξ_p^o for all poles as shown in Equations (24) and (25).

$$\chi^o=\sum_{p=1}^{N}\chi_p^o=\sum_{p=1}^{N}A_p\left[1-e^{-\frac{\Delta t}{\tau_p}}\right] \quad (24)$$

$$\xi^o=\sum_{p=1}^{N}\xi_p^o=-\sum_{p=1}^{N}A_p\frac{\tau_p}{\Delta t}\left[e^{-\frac{\Delta t}{\tau_p}}\left(\frac{\Delta t}{\tau_p}+1\right)-1\right] \quad (25)$$

Substituting from (22) and (23) into (15) and (16), respectively, at $m=0$ for each pole, one obtains

$$\Delta\chi_p^o=A_p\left[1-e^{-\frac{\Delta t}{\tau_p}}\right]^2, \quad (26)$$

$$\Delta\xi_p^o=-A_p\frac{\tau_p}{\Delta t}\left[1-e^{-\frac{\Delta t}{\tau_p}}\right]\left[e^{-\frac{\Delta t}{\tau_p}}\left(\frac{\Delta t}{\tau_p}+1\right)-1\right] \quad (27)$$

Using the relations (26) and (27) and manipulating the resulting equations as outlined in [11], the recursion relation for ψ^n for the pth pole is

$$\psi_p^n = \left(\Delta\chi_p^o - \Delta\xi_p^o\right) E^n + \Delta\xi_p^o E^{n-1} + e^{\frac{-\Delta t}{\tau_p}} \psi_p^{n-1} \tag{28}$$

For Equation (28), all the quantities are real-valued.

The recursive accumulator in the electric field update Equation (19) is the summation of the recursive accumulators of all poles

$$\psi^n = \sum_{P=1}^{N} \psi_p^n \tag{29}$$

As mentioned above, the dispersive properties of the soil used in this paper is described by the two-term Debye model, thus we can evaluate the parameters used in (19) for electric field computation as follows

$$\chi^o = A_1 \left[1 - e^{-\frac{\Delta t}{\tau_1}}\right] + A_2 \left[1 - e^{-\frac{\Delta t}{\tau_2}}\right] \tag{30}$$

$$\xi^o = -A_1 \frac{\tau_1}{\Delta t} \left[e^{-\frac{\Delta t}{\tau_1}} \left(\frac{\Delta t}{\tau_1} + 1\right) - 1\right] - A_2 \frac{\tau_2}{\Delta t} \left[e^{-\frac{\Delta t}{\tau_2}} \left(\frac{\Delta t}{\tau_2} + 1\right) - 1\right] \tag{31}$$

$\Delta\chi_1^o$, $\Delta\xi_1^o$ and $\Delta\chi_2^o$, $\Delta\xi_2^o$ are used to get ψ_1^n and ψ_2^n, respectively, using (28) and the total recursive accumulator can be evaluated as

$$\psi^n = \psi_1^n + \psi_2^n \tag{32}$$

Regarding the incorporation of this method into the original FDTD algorithm, the algorithm is programmed in the following order. At each time step, the electric field from the previous time step E^n is stored in a temporary variable, and the electric field is updated using (19). The recursive accumulator for the next time step $n+1$ is computed for each pole via (28) using E^{n+1} and E^n. Then the total recursive accumulator needed for the electric field update Equation (19) is computed using (32). The value of the recursive accumulator is zero at $n = 0$. Noteworthy, the FDTD update equations for the magnetic field remain unchanged from those normally used in [17].

3. NUMERICAL RESULTS

The PLRC method which has been modified as described above to deal with N-order Debye media is applied here to detect the existence of variety of targets buried in different types of dispersive soils. Before applying the modified PLRC method to solve such GPR problems, it is first examined by solving a problem of evaluating the electric field inside a half-space dispersive medium due to a radiating dipole

located in the free space region above this medium. To get the result of this examination significant we consider the same problem solved in [18] using the PML-PLRC-FDTD (Perfectly matched layer-PLRC-FDTD)approach based on the split form of Maxwell's equations and compare the results. The electric field is plotted at a point inside a medium with dispersive properties described by a two-term Debye model in a half-space problem. The radiating antenna is a y-directed infinitesimal electric dipole and the interface plane between the half-space medium and the free space region is the zx plane. The antenna is excited with the first derivative of Blackmann-Harris pulse shown in Figure 1 and given by the following equation [19]

$$f(t) = 2 * 10^5 \begin{cases} \sum_{n=0}^{3} a_n \cos\left(\frac{2\pi nt}{T}\right), & 0 < t < T \\ 0, & \text{else} \end{cases} \tag{33}$$

where $T = 1.55/f_c$ is the pulse period, $f_c = 200\,\text{MHz}$ is the center frequency of the pulse and $a_0 = 0.35322222$, $a_1 = -0.488$, $a_2 = 0.145$, $a_3 = -0.010222222$ are the function coefficients.

The simulation domain is taken to be $50 \times 50 \times 50$ cubic-cell-lattice with spatial increment of $\Delta = 5.86\,\text{cm}$ and time step of $\Delta = 90.2\,\text{ps}$. The dispersive material occupies 60% of the vertical dimension of the simulation domain and the dispersion properties are taken for Puerto-

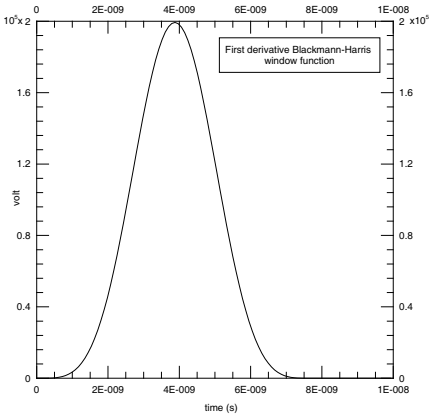

Figure 1. First derivative Blackmann-Harris pulse as a source for the transmitting dipole in example 1.

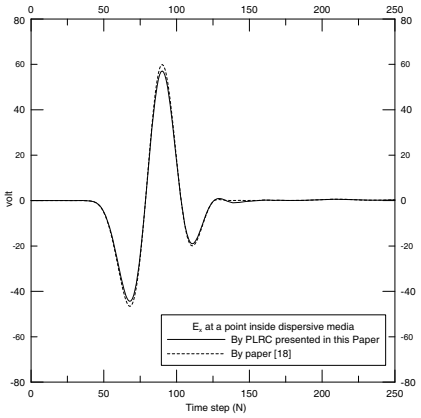

Figure 2. E_x at a point inside the dispersive half-space in example 1 using the formulation developed in this paper compared with the solution of [18].

Table 1. Two-term Debye model parameters for Puerto Rico-type clay loams [18].

Moisture content	ε_∞	A_1	A_2	τ_1 (nsec)	τ_2 (nsec)	σ (mS/m)
2.5 %	3.20	0.75	0.30	2.71	0.108	0.397
5%	4.15	1.80	0.60	3.79	0.151	1.11
10%	6.00	2.75	0.75	3.98	0.251	2.00

Rico clay loams with 5% moisture content [18] as given in Table 1. The antenna is located at $(25 \times 35 \times 25)\Delta$ (assuming the origin of the grid at lower left corner). The x-component of the electric field (E_x) at a point inside the dispersive soil computed by the modified approach presented in this paper is plotted in Figure 2 in comparison with that of [18]. It is noticeable that both results are in a very good agreement.

The dispersive model presented in this paper is employed in some cases of buried object detection where the soil has two-term Debye model. The computation domain in the first case is discretized as $N_x \times N_y \times N_z = 80 \times 100 \times 70$ grid and is divided into two parts the upper part is the free-space including the GPR system and the lower part is the ground soil including the buried object. The space increment is $\Delta = 0.752\,\text{cm}$, the time increment is $\Delta t = 14.472\,\text{ps}$ and the Courant stability factor is set to $S = 1$. The run time takes 4000 time steps to ensure reaching the steady state condition. An 8-cell UPML (Uniaxial Perfectly Matched Layer) is used to terminate the simulation domain. The part of the UPML interfacing the free-space region has a relative permittivity of unity, whereas the part of the UPML interfacing the soil region has a relative permittivity equal to the infinite-frequency permittivity ε_∞ of the dispersive model of the soil. The GPR antenna is composed of two half-wavelength dipoles; one is used as a transmitting antenna and the other as a receiving antenna. Both the transmitting and receiving dipoles are located just above the ground surface and directed parallel to x-axis. The dipoles are separated with a metallic wall of one-cell thickness modeled as a PEC (perfect electric conductor) extending between the two PML boundaries in the x-direction and from the PML limit to the surface of the ground in the z-direction. This wall is used to eliminate the direct coupling between the transmitting and receiving dipoles and to reduce the possibility of improper detection of buried target. Figure 3 shows the geometry of the system used in this example.

The transmitting dipole is fed with the differential Gaussian pulse

shown in Figure 4 and of the form:

$$V(t) = V_o \frac{(t_o - t)}{T^2} e^{\frac{-(t-t_o)^2}{2T^2}} \tag{34}$$

where, $V_o = 5 \times 10^{-6}\, V$ is a parameter proportional to the pulse amplitude, $t_o = 2.96\,\text{ns}$ is the instant of time at the center of the pulse and $T = 300\,\text{ps}$ is proportional to the pulse width. The choice of these parameters results in the signal spectrum shown in Figure 5, which is obtained by the discrete Fourier transform.

The dipoles are of length 28.85 cm which is equivalent to the half-wavelength at the central frequency of the excitation pulse (520 MHz). Both the transmitting and receiving dipoles are located just above the ground surface. The buried target is a Plexiglas block with relative electric permittivity $\varepsilon_r = 2.6$ and dimensions of $(30.08 \times 49.63 \times 6.77)\,\text{cm}^3$. The block is buried in the Puerto-Rico type clay loams at 15 cm below earth surface. The model parameters for the simulation with dispersion are taken from Table 1 for the Puerto-Rico clay loams with 10% moisture content. The constitutive parameters of the simulation without dispersion are taken for the relative permittivity to be $\varepsilon_r = \varepsilon_\infty = 6.0$ [13] and for the electric conductivity to be $\sigma = 2.0\,\text{mS/m}$. The detection of block existence is determined by the difference in the transmission coefficient S_{21} (expressed in dB) as in Equation (35) in the presence and absence of the block.

$$S_{21} = 20\log_{10}(V_r/V_t) \tag{35}$$

where V_r is the voltage at the receiving antenna and V_t is the voltage at the transmitting antenna at the same frequency.

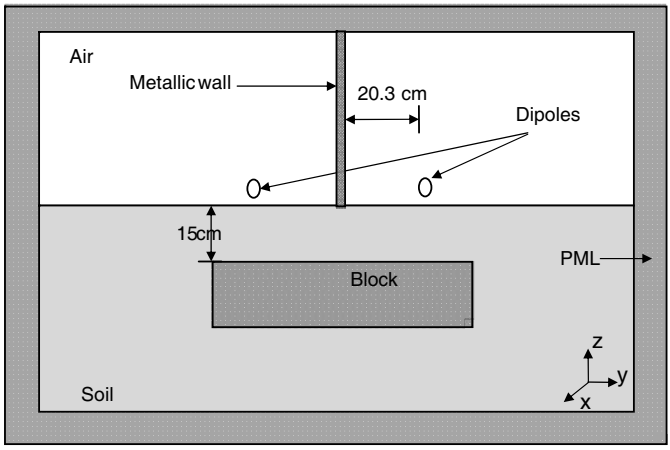

Figure 3. GPR system geometry employed in example 2.

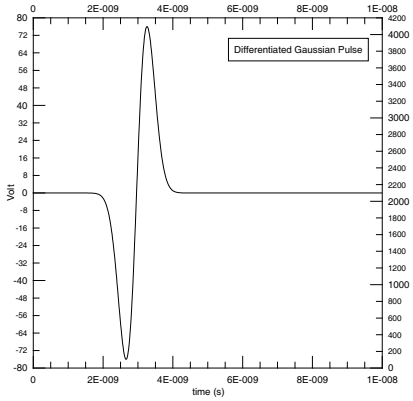

Figure 4. Differentiated Gaussian pulse as source for the transmitting dipole in the time domain.

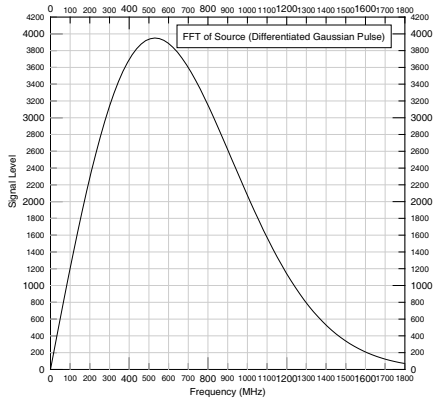

Figure 5. FFT of differentiated Gaussian pulse for the transmitting dipole.

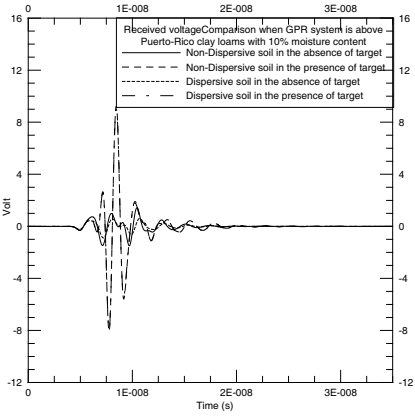

Figure 6. Comparison of received signal in time domain applying dispersive and non-dispersive models of the Puerto-Rico type clay soil in the presence and absence of a plexi-glass block.

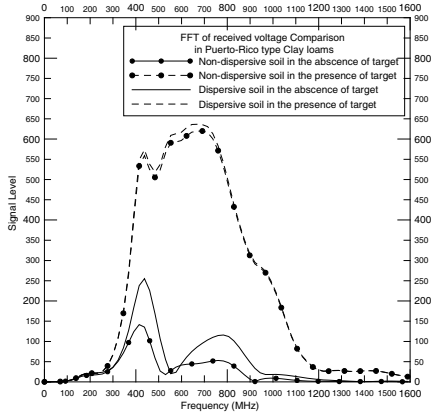

Figure 7. Comparison of received signal in frequency domain applying dispersive and non-dispersive models of the Puerto-Rico type clay soil in the presence and absence of a plexi-glass block.

Comparisons between the values of the received signals in the cases of the presence and absence of a buried target and, also, in the cases of employing dispersive and non-dispersive models of the ground soil are shown in Figures 6 and 7. It is noticed that the

received signal is increased due to the presence of the buried target. The reason behind this is that the transmitted wave is guided by the block which occupies a considerable volume of the ground region. As clear from Figure 6, curves representing the received voltage in the case of the presence of the block in both cases of employing the dispersive and non-dispersive model of soil are approximately coincide. This is because the buried block occupies a reasonable volume of the ground region. The field calculation in this region is performed using the standard scheme of the FDTD since the block is considered non-dispersive. Figure 8 shows the variation of the coupling parameter S_{21} defined by (35) in the same cases. As clear from Figure 8, there is a significant increase in the values of S_{21} due to the presence of the buried block for both cases of dispersive and non-dispersive of soils. Considering the effect of employing the dispersive model for the ground soil instead of the non-dispersive model on the obtained results, we notice that, at low frequencies (up to 200 MHz) there is no noticeable differences between the values obtained for S_{21} in the two cases. This is because electrical permittivity and conductivity of the ground are approximately constant and frequency independent in the low frequency range. On the other hand, the higher frequency range shows that more deviation of the obtained results in the case

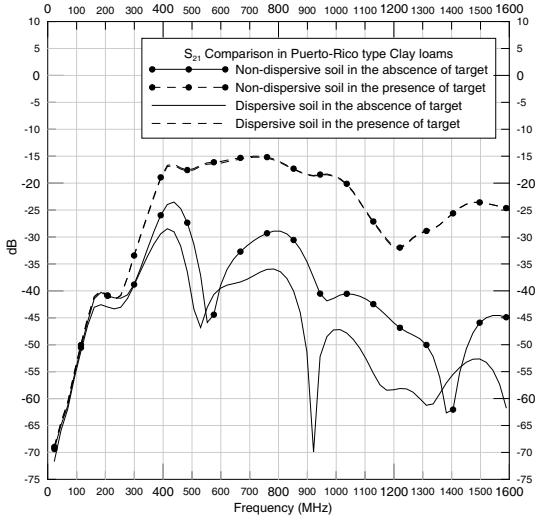

Figure 8. Comparison of S_{21} applying dispersive and non-dispersive models of the Puerto-Rico type clay soil in the presence and absence of a plexi-glass block.

of a dispersive soil model from that of the non-dispersive one due to the stronger dependence of the dispersive model parameters on the frequency in this range.

The electromagnetic fields are computed using the ordinary update equations that do not include a dispersive model for the soil, where Figures 9 and 10 show some time-domain snap-shots for the electric field intensity distributions around the dipoles, and in the ground soil during the process of block detection. Figures 11 and 12 show the corresponding snap-shots when a dispersive soil model is employed. By comparing the field distributions shown in Figures 9 and 11 to those of Figures 10 and 12 respectively, it is noticed that the wave fronts of the field at the region of the ground at the block position when it is present, are different from those in an empty soil. This is attributed to that the permittivity of the target is lower than that of the ground which leads to larger distances between the wave fronts inside the block region when it is present.

The next case of buried target detection to be studied is to show the impact of the soil moisture content on the performance of the same GPR system utilized in the last case. The simulation parameters and system dimensions are kept the same as those in the last case except for the moisture content percentage of the Puerto-Rico type clay loams. Three different percentages of soil moisture are used (2.5%, 5%, and 10%) with the same plexi-glass block buried at the same depth.

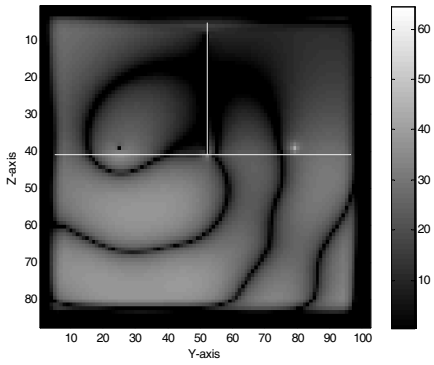

Figure 9. Electric field intensity distribution in Puerto-Rico clay soil (using non-dispersive model) and around the GPR system in the absence of a buried block.

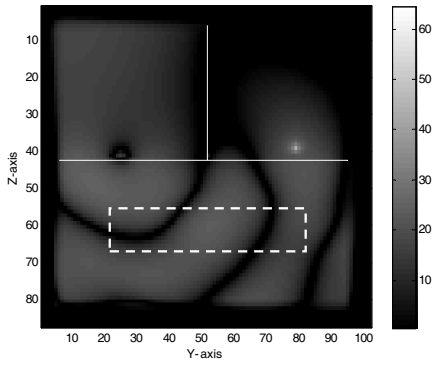

Figure 10. Electric field intensity distribution in Puerto-Rico clay soil (using non-dispersive model) and around the GPR system in the presence of a buried block.

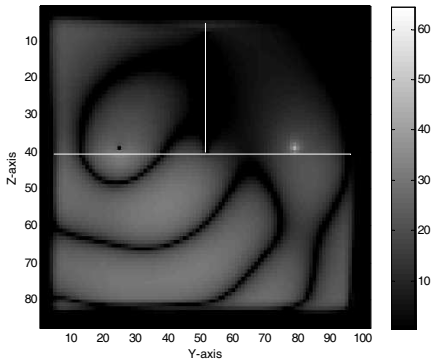

Figure 11. Electric field intensity distribution in Puerto-Rico clay soil (using dispersive model) and around the antennas of the GPR system in the absence of a buried block.

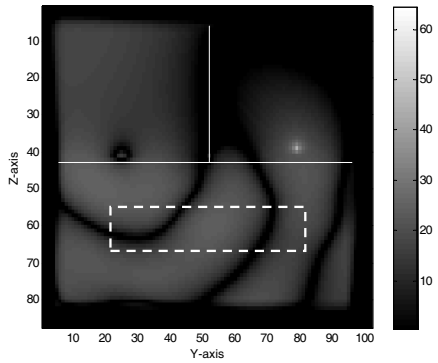

Figure 12. Electric field intensity distribution in Puerto-Rico clay soil (using dispersive model) and around the antennas of the GPR system in the presence of a buried block.

In the time domain, Figure 13 shows the received signal voltage at the receiving dipole in the cases of the absence and the presence of the buried block. The amplitude of the received voltage increases due to waves' reflection from the buried block. This is also shown in Figure 14 when the received voltage is Fourier transformed in the frequency band (500–1100 MHz). Figure 15 shows a plot of the coupling coefficient in the case of a plexi-glass block buried in the Puerto Rico clay soil with 2.5% moisture content compared with that in the case when the soil is empty. It is clear that the difference in the S_{21} due to the existence of the block is a few decibels over the frequency band (500–1100 MHz). This difference is relatively small and may not be enough to give a clear detection of the block. This small difference in S_{21} may be attributed to the low contrast between the soil and the buried block at this moisture content ($\varepsilon_\infty = 3.2$ for the soil versus 2.6 for the block) as listed in Table 1.

Figures 16, 17 and 18 show that increasing the moisture content of the soil to 5% leads to a significant increase in the received signal as well as the coupling coefficient compared to the results obtained when the moisture content of soil is 2.5%. Figure 18 shows that the difference in coupling coefficient is enhanced to be within the range (10–25) dB over the frequency band (450–1100) MHz which increases the possibility of detecting the buried. Figures 16 and 17 show that the received signal level (both in the time and frequency domains) due

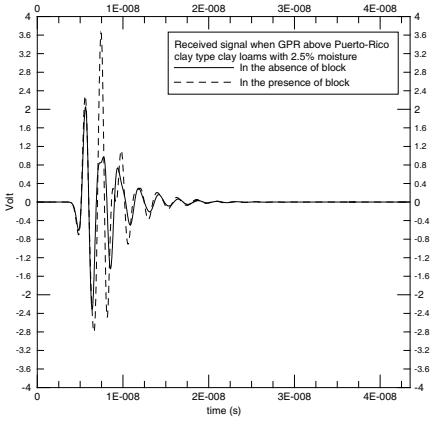

Figure 13. The received signal level with time when the GPR system is located above the dispersive Puerto-Rico type clay soil with 2.5% moisture content in the presence and absence of the plexi-glass block.

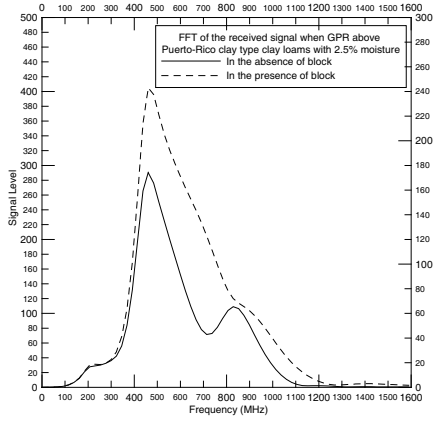

Figure 14. FFT of the received signal when the GPR system is located above the dispersive Puerto-Rico type clay soil with 2.5% moisture content in the presence and absence of the plexi-glass block.

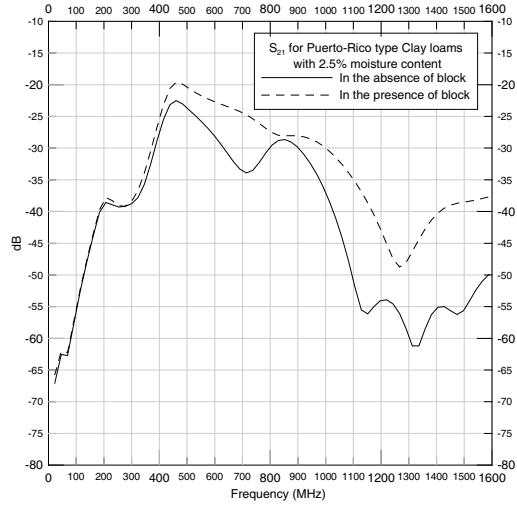

Figure 15. S_{21} when the GPR system is located above the dispersive Puerto-Rico type clay soil with 2.5% moisture content in the presence and absence of the plexi-glass block.

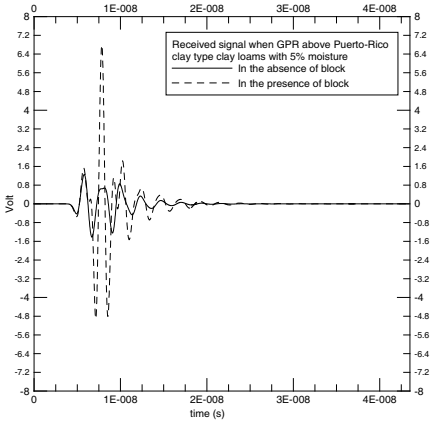

Figure 16. The received signal level with time when the GPR system is located above the dispersive Puerto-Rico type clay soil with 5% moisture content in the presence and absence of the plexi-glass block.

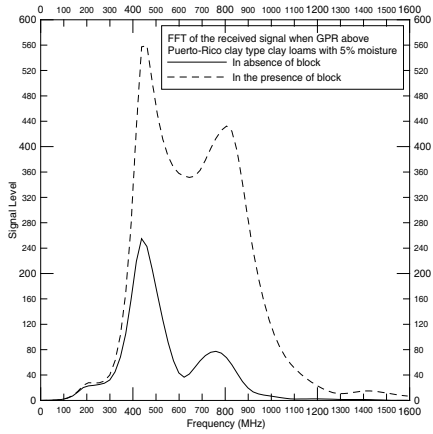

Figure 17. FFT of the received signal when the GPR system is located above the dispersive Puerto-Rico type clay soil with 5% moisture content in the presence and absence of the plexi-glass block.

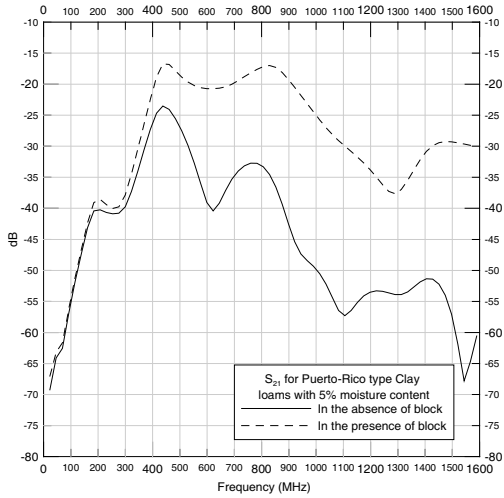

Figure 18. S_{21} when the GPR system is located above the dispersive Puerto-Rico type clay soil with 5% moisture content in the presence and absence of the plexi-glass block.

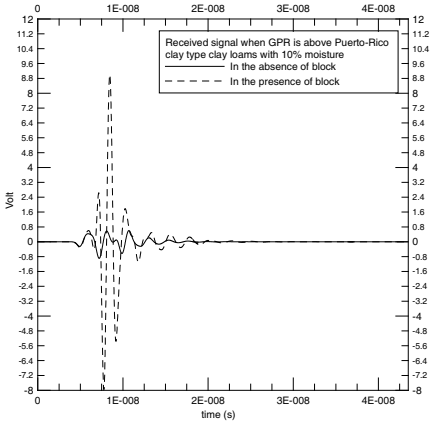

Figure 19. The received signal level with time when the GPR system is located above the dispersive Puerto-Rico type clay soil with 10% moisture content in the presence and absence of the plexiglass block.

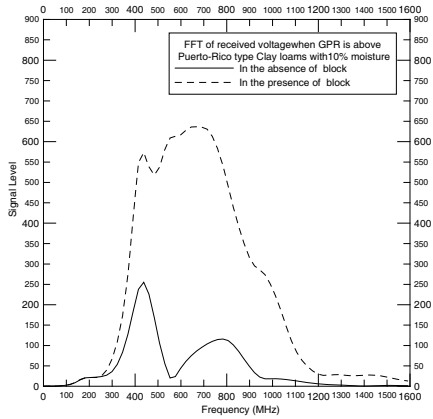

Figure 20. FFT of the received signal when the GPR system is located above the dispersive Puerto-Rico type clay soil with 10% moisture content in the presence and absence of Plexiglas block.

to the presence of block is nearly four times the received signal level in the case of an empty soil.

When the moisture percentage is raised to 10% in the Puerto-Rico type clay soil, the ability of block detection increases in comparison to the previous cases of soils with 2.5% and 5% moisture contents. In the time domain, it is noticeable from Figures 19 and 20 that the amplitude of received signal level in the presence of the buried block is about eleven times more than that in the absence of the target. As appearing in Figure 21, the presence of the buried block leads to increase the value of S_{21} by about 10 dB over the frequency range (380–450 MHz) and by more than 25 dB over almost all the higher frequencies in operating band. This can be attributed to the high contrast between the permittivity of soil with 10% moisture and that of the buried block (6 versus 2.6).

The third case to be investigated demonstrates the effect of the soil properties on the GPR system capability of detection of buried pipes. Two types of soils are considered: Puerto-Rico clay soil and San Antonio clay soil with 10% moisture content, where the soil properties are shown in Tables 1 and 2, respectively. The same GPR system described in the last case is employed here with some modifications related to the wall thickness and the distances between the wall and

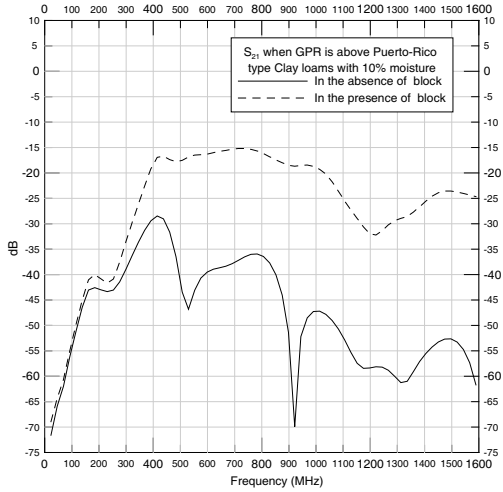

Figure 21. S_{21} when the GPR antenna is located above the dispersive Puerto-Rico type clay soil with 10% moisture content in the presence and absence of the plexi-glass block.

Table 2. Two-term Debye model parameters for San Antonio clay soil [20].

Moisture content	ε_∞	A_1	A_2	τ_1 (nsec)	τ_2 (nsec)	σ (mS/m)
2.5 %	3.635	1.667	0.482	1.70	0.120	1.40
5%	4.589	2.725	1.045	1.85	0.158	8.50
10%	6.310	6.150	1.685	2.30	0.174	22.00

the dipoles as shown in Figure 22. The space domain is divided as $77 \times 73 \times 120$ grid with a space increment of $\Delta = 0.752$ cm and time increment of $\Delta t = 14.472$ ps. The run time takes 3000 time steps to ensure reaching the steady state condition. The study involves the detection of solid metallic as well as plastic pipes buried in both types of the soil. The pipe diameter is 18.8 cm and it is placed so that the pipe axis is parallel to that of the dipole antenna and extends between the two PML internal sides parallel the x-axis to simulate a very long pipe with respect to the GPR antenna dimensions. Furthermore, the cross section of the pipe is modeled in the FDTD algorithm using the staircase approximation. The pipe is buried at a depth of 20.3 cm below the ground surface. The pipe is located right under the metallic wall separation between the transmitting and receiving dipoles as shown in Figure 22.

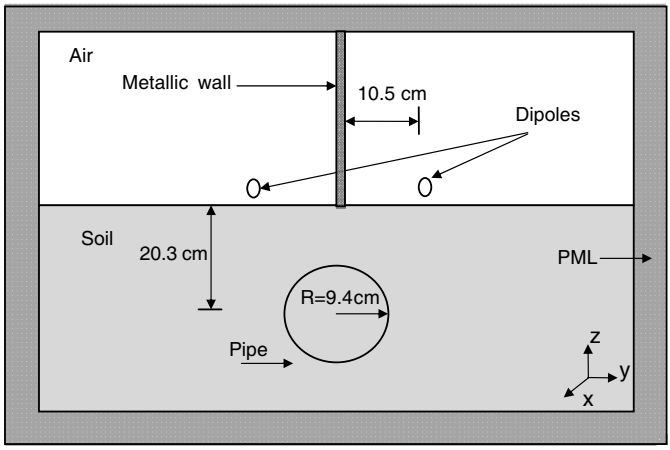

Figure 22. GPR system used for buried pipe detection.

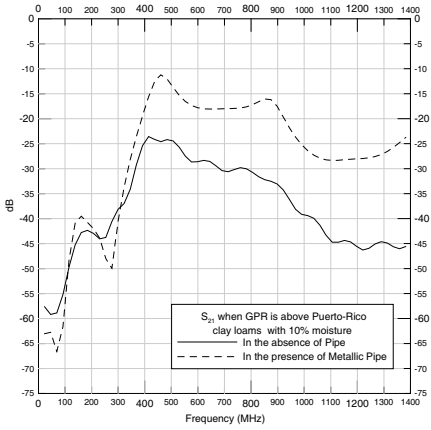

Figure 23. S_{21} when the GPR system is located above Puerto-Rico type clay soil with 10% moisture content in the presence and absence of a metallic pipe.

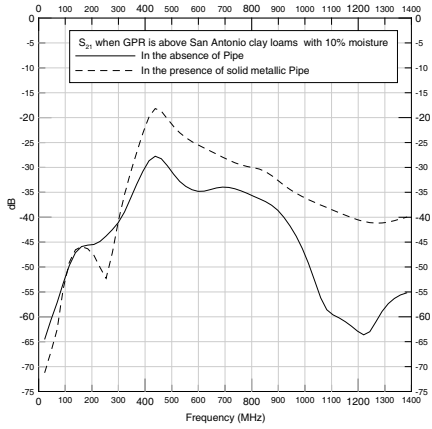

Figure 24. S_{21} when the GPR system is located above San Antonio clay soil with 10% moisture content in the presence and absence of a metallic pipe.

Figure 23 shows the transmission coefficient S_{21} for the detection of a metallic pipe (modeled as PEC) buried in a Puerto-Rico clay soil. It is clear that the buried pipe can be detected over the frequency band (450–1100 MHz) where coupling coefficient S_{21} increases by about 15 dB due to the existence of the pipe. On the other side, when the

same metallic pipe is buried at the same depth in San Antonio soil, the presence of the buried pipe leads an increase of about 10 dB in S_{21} over the same frequency band as shown in Figure 24. The increase of soil conductivity in the case of San Antonio clay soil contributes to the electromagnetic wave absorption and hence, which leads to decrease the strength of the received signal. As demonstrated in Figures 25 and 26, the amplitude of the received signal level in the case of San Antonio clay soil is significantly smaller than that in the case of Puerto-Rico clay soil.

The next case to be treated is to investigate the GPR target performance when the metallic pipe, considered in the last case is replaced by a solid plastic pipe with a relative permittivity of 2.0. Figures 27 and 28 show the coupling coefficient in the case of the absence and presence of the pipe when the GPR system is placed over Puerto-Rico soil and San Antonio soil, respectively. Although the ability of detection of the plastic pipe is weak in both soils due to the poor reflective nature of dielectrics, the difference in the coupling coefficient due to the presence of pipe in Puerto-Rico soil is bigger than that in San Antonio soil. This is due to the higher conductivity of San Antonio soil over that of Puerto-Rico soils at the same moisture

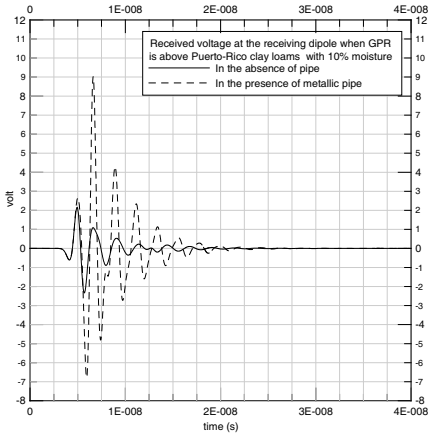

Figure 25. Comparison of the received signal level when the GPR system is located above Puerto-Rico type clay soil with 10% moisture content in the presence and absence of a metallic pipe.

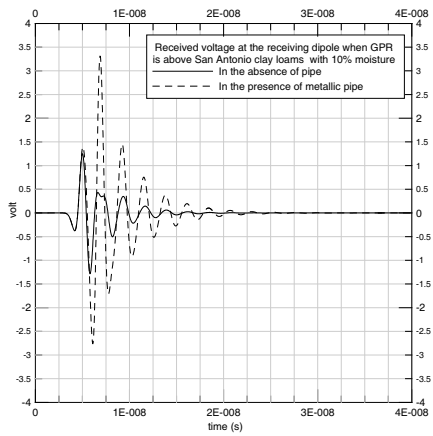

Figure 26. Comparison of the received signal level when the GPR antenna is located above San Antonio clay soil with 10% moisture content in the presence and absence of a metallic pipe.

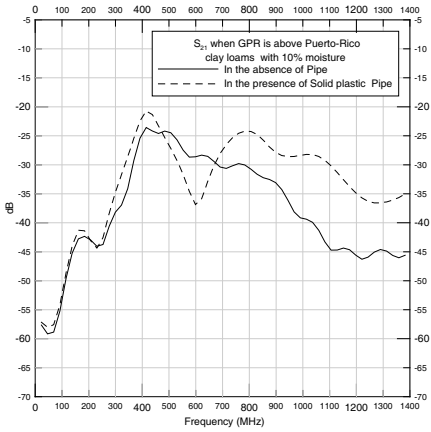

Figure 27. S_{21} when the GPR system is located above Puerto-Rico type clay soil with 10% moisture content in the presence and absence of a solid plastic pipe.

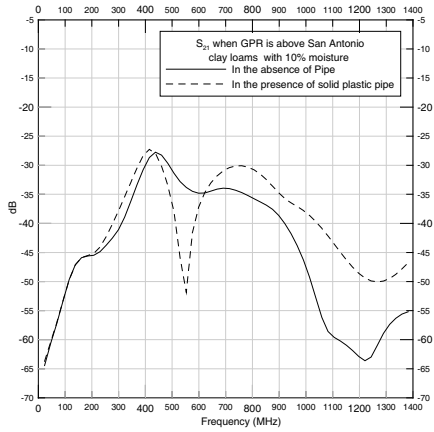

Figure 28. S_{21} when GPR system is located above San Antonio clay soil with 10% moisture content in the presence and absence of a a solid plastic pipe.

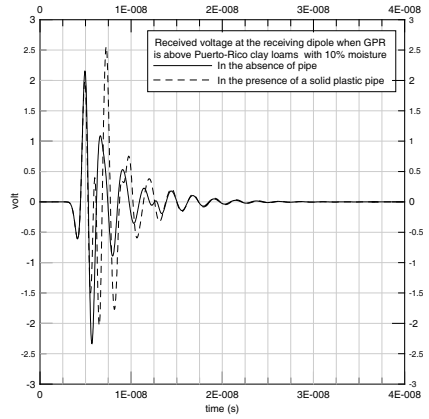

Figure 29. Comparison of the received signal level when the GPR system is located above Puerto-Rico type clay soil with 10% moisture content in the presence and absence of solid plastic pipe.

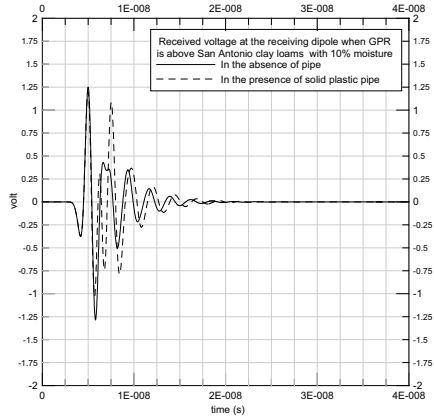

Figure 30. Comparison of the received signal level when the GPR system is located above San Antonio clay soil with 10% moisture content in the presence and absence of a solid plastic pipe.

content. As noticed from Figures 29 and 30, the amplitude of the received signal in the case of the presence of the pipe is close to that in the absence of pipe when buried in both soils.

Figures 31, 33 and 35 show time-domain snapshots for the electric field intensity distribution around the GPR antennas and in the Puerto-Rico clay loams during the process of pipe detection. It is clear, in these figures that there is a difference in the field distributions at the location of pipe and in the surrounding region because of the existence

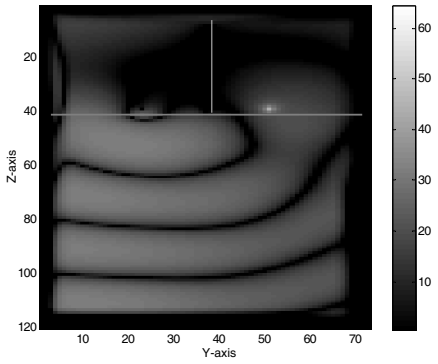

Figure 31. Electric field intensity distribution in Puerto-Rico clay soil and around the antennas in the absence of pipe.

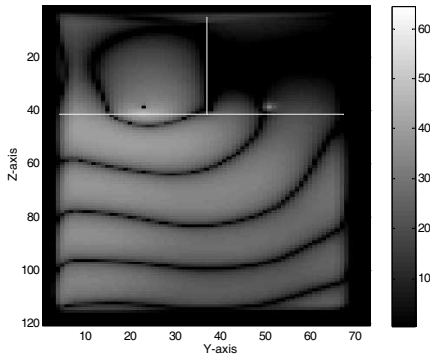

Figure 32. Electric field intensity distribution in San Antonio clay soil and around the antennas of the GPR system in the absence of the pipe.

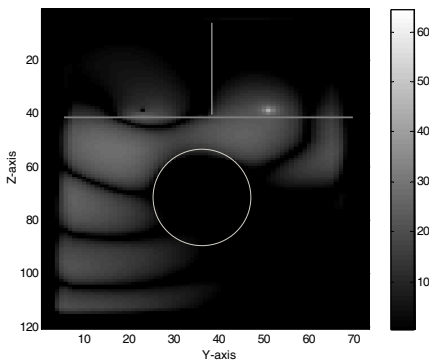

Figure 33. Electric field intensity distribution in a Puerto-Rico clay soil and around the antennas of the GPR system in the presence of a metallic pipe.

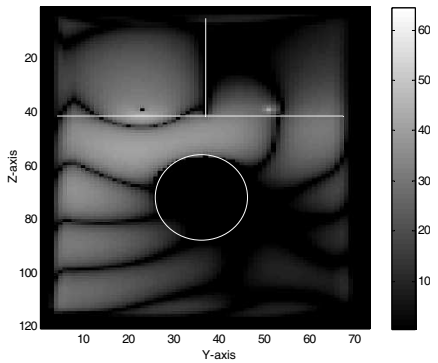

Figure 34. Electric field intensity distribution in a San Antonio clay soil and around the antennas of the GPR system in the presence of a metallic pipe.

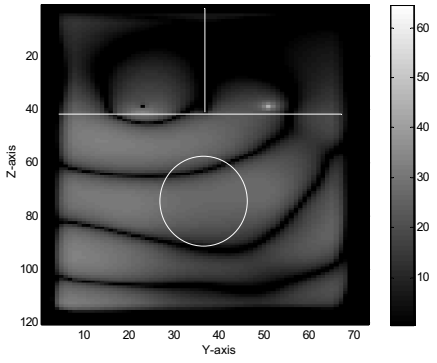

Figure 35. Electric field intensity distribution in a Puerto-Rico clay soil and around the antennas of the GPR system in the presence of a plastic Pipe. The metallic wall separating the dipoles and the Interface between the soil and the air regions are indicated by white lines.

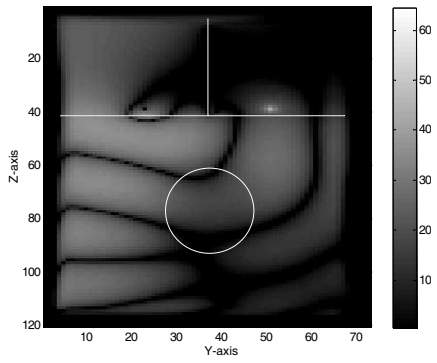

Figure 36. Electric field intensity distribution in a San Antonio clay soil and around the antennas of the GPR system in the presence of a plastic pipe.

of either the metallic pipe (where the tangential electric field is zero at its surface) or the plastic pipe (since the relative permittivity of the plastic pipe is much different from that of the surrounding soil). Other snapshots are taken for the San Antonio clay soil during the detection of the metallic and plastic pipes as those shown in Figures 32, 34, and 36. It is noticeable that the wave fronts of the wave in the San Antonio soil and at the pipe position are different from those appearing in Puerto-Rico soil because of the difference in the electrical properties between the two types of soil.

4. CONCLUSION

The incorporation of media dispersion into the ordinary FDTD algorithm is conducted in this paper in order to get more realistic modeling of practical soils. Three dimension PLRC-FDTD algorithm is formulated to model the dispersive soil characteristics as a two-term Debye medium. The validity of such an algorithm is proven by the comparison of the obtained results with other published ones. This algorithm is employed for the simulation of a simple GPR system for the detection of different objects (plexi-glass block, metallic and plastic pipes) buried in different types of dispersive soils with practical parameters. The effect of the soil moisture content on its properties

and hence on the capability of a GPR system to detect buried targets is studied. It is demonstrated that the higher contrast between the object and soil permittivity results in better capability of GPR systems to detect the buried target. Finally, the GPR system performance to detect the pipes buried in two different types of soil (Puerto-Rico and San Antonio) is studied. It is shown that as the soil permittivity and conductivity are increased the buried target detection becomes more difficult for GPR systems.

REFERENCES

1. Yee, K. S., "Numerical solution of initial boundary value problems involving Maxwell's equations in isotropic media," *IEEE Trans. Antennas Propagat.*, Vol. 14, 302–307, May 1966.
2. Bourgeois, J. M. and G. S. Smith, "A fully three-dimensional simulation of a ground-penetrating radar: FDTD theory compared with experiment," *IEEE Trans. Geosci. Remote Sensing*, Vol. 34, 36–44, Jan. 1996.
3. Gurel, L. and U. Oguz, "Simulations of ground penetrating radars over lossy and heterogeneous grounds," *IEEE Trans. Geosci. Remote Sensing*, Vol. 39, 1190–1197, Jun. 2001.
4. Montoya, T. P. and G. S. Smith, "Landmine detection using a ground-penetrating radar based on resistively loaded Vee dipoles," *IEEE Trans. Antennas Propagat.*, Vol. 47, 1795–1806, Dec. 1999.
5. Nishioka, Y., O. Maeshima, T. Uno, and S. Adachi, "FDTD analysis of resistor-loaded bow-tie antennas covered with ferrite-coated conducting cavity for subsurface radar," *IEEE Tarns. Antennas Propagat.*, Vol. 47, 970–997, Jun. 1999.
6. Young, J. L., "Propagation in linear dispersive media: Finite difference time-domain methodologies," *IEEE Trans. Antennas Propagat.*, Vol. 43, 422–426, 1995.
7. Sullivan, D. M., "Frequency-dependent FDTD methods using Z transforms," *IEEE Trans. Antennas Propagat.*, Vol. 40, 1223–1230, Oct. 1992.
8. Gandhi, O. P., B.-Q. Gao, and J.-Y. Chen, "A frequency-dependent finite difference time-domain formulation for general dispersive media," *IEEE Trans. Microwave Theory Technol.*, Vol. 41, 658–664, Apr. 1993.
9. Kashiva, T., Y. Ohtomo, and I. Fukai, "A finite-difference time-domain formulation for transient propagation in dispersive media associated with Cole-Cole's circular arc law," *Microwave. Opt. Technol. Lett.*, Vol. 3, No. 12, 416–419, 1990.

10. Joseph, R. M., S. C. Hagness, and A. Taflove, "Direct time integration of Maxwell's equations in linear dispersive media with absorption for scattering and propagation of femtosecond electromagnetic pulses," *Opt. Lett.*, Vol. 16, 1412–1414, 1991.
11. Luebbers, R. J., F. P. Huusberger, K. S. Kunz, R. B. Standler, and M. Schneider, "A frequency-dependent finite-difference time-domain formulation for dispersive materials," *IEEE Trans. Electromagn. Compat.*, Vol. 32, 1412–1414, Aug. 1990.
12. Luebbers, R. J. and F. P. Hunsberger, "FDTD for Nth-order dispersive media," *IEEE Trans. Antennas Propagat.*, Vol. 40, 1297–1301, Nov. 1992.
13. Luebbers, R. J., F. P. Hunsberger, and K. Kunz, "A frequency-dependent finite-difference time-domain formulation for transient propagation in plasma," *IEEE Trans. Antennas Propagat.*, Vol. 39, 29–39, 1991.
14. Sullivan, D. M., "A frequency-dependent FDTD method for biological applications," *IEEE Trans. Microwave Theory Tech.*, Vol. 40, 532–539, Mar. 1992.
15. Kelley, D. F. and R. J. Luebbers, "Piecewise linear recursive convolution for dispersive media using FDTD," *IEEE Trans. Antennas Propagat.*, Vol. 44, 792–797, 1996.
16. Weedon, W. H. and C. M. Rappaport, "A general method for FDTD modeling of wave propagation in arbitrary frequency-dispersive media," *IEEE Trans. Antennas Propagat.*, Vol. 45, No. 3, 401–410, Mar. 1997.
17. Taflove, A., *Computational Electromagnetics: The Finite-difference Time-domain Method*, Artech House, Boston, MA, 2000.
18. Teixeira, F. L., W. C. Chew, M. Straka, M. L. Oristaglio, and T. Wang, "Finite-difference time-domain simulation of ground penetrating radar on dispersive, inhomogeneous, and conductive soils," *IEEE Trans. Geos. and Remot. Sensing*, Vol. 36, No. 6, 1928–1937, Nov. 1998.
19. Lu, T., W. Cai, and P. Zhang, "Discontinuous galerkin time-domain method for GPR simulation in dispersive media," *IEEE Trans. Geos. and Remot. Sensing*, Vol. 43, No. 1, 72–80, Jan. 2005.
20. Uduwawala, D., M. Norgren, P. Fuks, and A. W. Gunawardena, "A complete FDTD simulation of a real GPR antenna system operating above lossy and dispersive grounds," *Progress In Electromagnetics Research*, Vol. 50, 209–229, 2005.